Journal of Nuclear Materials 377 (2008) 449–457

Contents lists available at ScienceDirect

Journal of Nuclear Materials

journal homepage: www.elsevier.com/locate/jnucmat

Actinide burner fuel: Potential compositions based on the thermodynamic evaluation of MF–PuF_3 (M = Li, Na, K, Rb, Cs) and LaF_3–PuF_3 systems

O. Beneš *, R.J.M. Konings

European Commission, Joint Research Centre, Institute for Transuranium Elements, P.O. Box 2340, 76125 Karlsruhe, Germany

ARTICLE INFO

Article history:
Received 22 February 2008
Accepted 7 April 2008

ABSTRACT

In previous studies a thermodynamic description of the LiF–NaF–KF–RbF–CsF–LaF_3 system was presented. In order to add PuF_3 to this system the assessments of LiF–PuF_3, NaF–PuF_3, KF–PuF_3, RbF–PuF_3, CsF–PuF_3 and LaF_3–PuF_3 binary phase diagrams have been made. In case of the LiF–PuF_3 and NaF–PuF_3 the assessments have been based on known experimental data. The other binary systems have not been measured yet and the thermodynamic description has been made using the excess parameters from the previously assessed binaries containing LaF_3, which is considered as a proxy compound for PuF_3. The main aim of this study is to analyze potential compositions for a molten salt fast burner fuel.

1. Introduction

The molten salt reactor (MSR) is one of the six nuclear concepts of the Generation IV initiative. The fuel of the MSR consists of a molten salt matrix in which the fissile material, such as ^{233}U, ^{235}U, ^{239}Pu or higher actinides, is dissolved in form of tri- or tetrahalides. A big advantage of this concept is the possibility of fuel clean-up during the operation. This fact increases the efficiency of the reactor, because the fission products with parasitic neutron capturing are continuously removed.

There are two main approaches in the MSR project. The first approach is based on a moderated thermal neutron spectrum and the highest interest in this type of reactor is for the breeder design based on the $^{232}Th/^{233}U$ cycle. In this case the matrix must be made from the materials with minimal neutron capture cross section and the $^{7}LiF–BeF_2$ system seems to be a very good candidate. The second approach is characterized by a non-moderated fast neutron spectrum which is of big interest for transmutation of plutonium and minor actinides. Such a concept is known as an Actinide Burner and the fuel will be most likely ^{239}Pu with small addition of minor actinides such as Np, Am and Cm. For a fast reactor the choice of the matrix material is not as limited as for a thermal reactor, because the neutron economy in the fast reactor is not as sensitive as in case of thermal spectrum, therefore compounds with higher neutron cross section in a given spectrum (like KF and RbF) can be part of the matrix. It is also worth to mention that better solubility for plutonium and other actinides is achieved when using the matrix based only on alkali metal halides [1,2].

The fuel choice is not only based on the neutronic properties and the solubility of the fissile material, but also on other aspects like melting temperature, vapor pressure, stability to radiation, viscosity or heat capacity. Because several of the above mentioned properties can be obtained from thermodynamic models, a thermodynamic description of the LiF–NaF–KF–RbF–CsF–LaF_3–PuF_3 system is presented in this study. Here the LiF–NaF is considered as a matrix, whereas KF and RbF are considered as components to lower the melting temperature. PuF_3 is the fissile material and CsF together with LaF_3 represent the fission products that are difficult to separate from the fuel during the clean-up treatment, and whose accumulation in the fuel matrix is expected.

In two previous studies [3,4] the thermodynamic assessment of the LiF–NaF–KF–RbF–CsF–LaF_3 system has been described. In this work the PuF_3 compound is added to the existing system. In order to do so, six binary phase diagrams had to be assessed. In case of the LiF–PuF_3 and NaF–PuF_3 systems this was done on a basis of known experimental data. In case of MF–PuF_3 (M = K, Rb, Cs) binary systems there are no experimental data known so these phase diagrams were calculated assuming the data from the MF–LaF_3 (M = K, Rb, Cs) assessments [3,4]. This is possible since LaF_3 is considered as a proxy compound to PuF_3. The last LaF_3–PuF_3 system was treated as ideal.

The main aim of this study is to analyze potential fuel compositions for an Actinide Burner concept. Based on our thermodynamic approach the prediction of its melting behavior, vapor pressure and the solubility of actinides has been made. Furthermore the fuel properties are compared to those of a fuel that is contaminated with some concentrations of the accumulated CsF and LaF_3 fission products.

* Corresponding author. Tel.: +49 7247 951263; fax: +49 7247 951566.
E-mail address: ondrej.benes@ec.europa.eu (O. Beneš).

0022-3115/$ - see front matter © 2008 Elsevier B.V. All rights reserved.
doi:10.1016/j.jnucmat.2008.04.004

2. Thermodynamic modelling

2.1. General approach

To describe a T–X phase diagram the Gibbs energy equations of all phases and the Gibbs equations of mixing, in case of the presence of solutions, are required. Thermodynamic data of most of the condensed phases were summarized in previous works [3,4], only the data for PuF_3 and for the intermediate phases containing Pu were not reported yet and are listed in Table 2. Data for PuF_3 have been taken from our internal report [5], the heat capacity and the absolute entropy at 298.15 K for $NaPuF_4$ (the only intermediate compound reported experimentally so far) from [6], while the enthalpy at 298.15 K had to be assessed in this work. None of the others intermediate phases containing Pu have been experimentally reported yet. Nevertheless they had to be included in this work in order to reproduce the phase diagrams correctly. Only the analogue intermediate compounds containing Pu as found in the MF–LaF_3 (M = Na, K, Rb, Cs) were taken into account. To derive their thermodynamic properties the Neumann–Kopp rule has been used to estimate the heat capacities. For enthalpies at 298.15 K and absolute entropies at 298.15 K the proportional weights of the end-member contributions were applied with addition of the reaction enthalpies and entropies, respectively. These reaction contributions were derived from the proxy intermediate compounds from the MF–LaF_3 (M = Na, K, Rb, Cs) systems [3,4]. For instance the thermodynamic data for a Rb_3PuF_6 were obtained as shown in Eqs. (1)–(3)

$$C_{p_{Rb_3PuF_6}}(T) = 3 \cdot C_{p_{RbF}}(T) + C_{p_{PuF_3}}(T), \tag{1}$$

$$\Delta_f H^0_{Rb_3PuF_6}(298.15\ \mathrm{K}) = 3 \cdot \Delta_f H^0_{RbF}(298.15\ K) + \Delta_f H^0_{PuF_3}(298.15\ \mathrm{K}) + \Delta_r H_{Rb_3LaF_6}, \tag{2}$$

$$S^0_{Rb_3PuF_6}(298.15\ \mathrm{K}) = 3 \cdot S^0_{RbF}(298.15\ \mathrm{K}) + S^0_{PuF_3}(298.15\ \mathrm{K}) + \Delta_r S_{Rb_3LaF_6}. \tag{3}$$

Table 1
Calculated solubility of PuF_3 in the mixtures of given initial composition

Matrix composition (mol%)	Solubility (mole fraction)	Temperature range (K)
LiF–KF (0.488–0.512)	$\log_{10}S = -1.211 + 0.733 \cdot 10^{-3} \cdot T$	843–1023
LiF–RbF (0.445–0.555)	$\log_{10}S = 53.144–1.3615 \cdot 10^{-1} \cdot T + 8.541 \cdot 10^{-5} \cdot T^2$ $\log_{10}S = -1.253 + 7.727 \cdot 10^{-4} \cdot T$	823–859 859–1023
LiF–NaF–RbF (0.400–0.142–0.458)	$\log_{10}S = 1.391–7.680 \cdot 10^{-3} \cdot T + 6.016 \cdot 10^{-6} \cdot T^2$ $\log_{10}S = -1.246 + 7.587 \cdot 10^{-4} \cdot T$	823–933 933–1023
LiF–NaF–KF (0.439–0.142–0.419)	$\log_{10}S = -1.416–2.670 \cdot 10^{-3} \cdot T + 3.859 \cdot 10^{-6} \cdot T^2$ $\log_{10}S = -1.160 + 6.768 \cdot 10^{-4} \cdot T$	823–938 938–1023
LiF–KF–RbF (0.434–0.190–0.376)	$\log_{10}S = -1.209 + 7.366 \cdot 10^{-4} \cdot T$	828–1023

Table 2
$\Delta_f H^0(298.15)$ (kJ mol^{-1}), $S^0(298.15)$ (J K^{-1} mol^{-1}) data and C_p (J K^{-1} mol^{-1}) coefficients for the pure components and intermediate compounds

Compound	$\Delta_f H^0_{(298.15)}$	$S^0_{(298.15)}$	a	$b\,T$	$c\,T^2$	$d\,T^{-2}$	Reference
PuF_3(s)	−1586.694	126.11	104.08	0.000707		−1035500	[5]
PuF_3(l)	−1568.813	109.33	130.00				[5]
$NaPuF_4$(s)	−2228.446	130.11	146.91	0.017736		−1132300	*
$KPuF_4$(s)[d]	−2166.700	192.66	172.84	−0.057050	7.5405E−5	−1802218	*
K_3PuF_6(s)[e]	−3316.012	325.75	310.35	−0.172564	2.2622E−4	−3335655	**
$RbPuF_4$(s)	−2163.749	201.70	146.42	0.026731		−1082400	**
Rb_2PuF_5(s)	−2713.050	299.56	188.76	0.052755		−1129300	**
Rb_3PuF_6(s)	−3292.575	361.67	231.11	0.078779		−1176200	**
Cs_3PuF_6(s)	−3363.963	391.01	244.51	0.053477		−1060165	**
PuF(g)	−112.600	251.00	36.64	0.000921	−1.4443E−7	−302540	[15]
PuF_2(g)	−614.300	297.00	57.31	0.000727	−1.4721E−7	−538960	[15]
PuF_3(g)[a,f]	−1167.800	336.11	81.61	−0.005210	1E−5	−771071	[15]
PuF_4(g)[b]	−1548.000	359.00	105.11	0.002841	−6.8873E−7	−1196830	[15]
PuF_6(g)[c]	−1812.700	368.90	143.99	0.023211	−1.0764E−5	−1834270	[15]
LiF(g)	−340.946	200.19	35.40	0.0018707	−1.6543E−7		[16]
Li_2F_2(g)	−935.323	261.80	83.09	1E−5		−2170730	[16]
Li_3F_3(g)	−1524.598	316.70	132.92	3E−5		−3747000	[16]
NaF(g)	−295.158	217.50	36.98	0.000789	1.2644E−7		[16]
Na_2F_2(g)	−834.063	297.79	83.14	2.1051E−6		−820673	[16]
KF(g)	−326.770	226.61	37.41	0.000690		−253835	[16]
K_2F_2(g)	−862.741	319.96	83.14	2.8338E−7		−436183	[16]
RbF(g)	−333.513	237.00	37.25	0.000616	1.4853E−7		[16]
Rb_2F_2(g)	−854.914	342.71	83.14	6.7819E−7		−384494	[16]
CsF(g)	−356.500	243.21	37.39	0.000570		−157082	[16]
LaF_3(g)	−1254.700	326.69	110.03	−0.033635	1.3634E−5		[16]

[a] Valid for temperature range 298.15–2800 K.
[b] Valid for temperature range 298.15–2400 K.
[c] Valid for temperature range 298.15–1000 K.
[d] An extra term in the C_p function: $-2.3886E{-}8T^3$.
[e] An extra term in the C_p function: $-7.1657E{-}8T^3$.
[f] An extra term in the C_p function: $-2.4612E{-}9T^3$.
** Neumann–Kopp rule for C_p, $S^0(298.15)$ and ΔfH^0 (298.15) derived using the reaction data from 'proxy' compounds containing La.
* C_p and $S^0(298.15)$ taken from [6], $\Delta_f H^0_{(298.15)}$ optimized in this study.

Since one of the goals of this study was to calculate the vapor pressure of the fuel, the gas phases of relevant fluorides had to be considered. Thermodynamic data of all the gas phases taken into account in this study are summarized in Table 2.

2.2. Liquid solutions

The modified quasi-chemical model [7,8] has been used to optimize the excess Gibbs parameters of the liquid solutions. In case of the LiF–PuF_3 and NaF–PuF_3 systems the experimental description is known [9,10] and these data have been used to optimize the phase diagrams. Since the quasi-chemical model has been explained by Chartrand and Pelton [7,8] and also rough descriptions have been shown in our previous works [3,4], the reader is referred to those publications for details. Only the optimized parameters and the coordination numbers are presented in Eqs. (4) and (5) and in Table 3 respectively. $\Delta g^0_{AB/F}$ in Eqs. (4)–(9), where A and B represent two different cations on one sublattice, is the Gibbs energy for the second nearest neighbor pair-exchange reaction, while $\chi_{AB/F}$ term is a composition variable

$$\Delta g_{LiPu/FF} = -2928.8 - 3347.2\chi_{PuLi}\ \mathrm{J\ mol^{-1}} \quad (4)$$

$$\Delta g_{NaPu/FF} = -16317.6 - 6276\chi_{PuNa} - 1673.6\chi_{NaPu}\ \mathrm{J\ mol^{-1}}. \quad (5)$$

For the other binary subsystems containing plutonium (KF–PuF_3; RbF–PuF_3; CsF–PuF_3; LaF_3–PuF_3) no experimental data are known and therefore no optimization of the phase diagrams is possible. In order to calculate these systems the excess Gibbs parameters for the liquid solutions as obtained from the similar systems containing LaF_3 from our previous work [4] have been used. For instance the excess Gibbs parameters for the KF–PuF_3 liquid solution correspond to the ones from the KF–LaF_3 system. The values for the binary excess data are listed in Eqs. (6)–(8). Since LaF_3 is considered as very similar compound to PuF_3 and because no experimental data nor proxy systems are known in case of LaF_3–PuF_3, the (La,Pu)F liquid solution has been treated as ideal. It must be noted that the third coefficient in Eq. (7) is lower than the one for RbF–LaF_3 system presented in previous study [3]. This is due to the fact that the RbF–LaF_3 system has been slightly reoptimized in order to better fit the liquidus line through the experimental points on the RbF rich side (Fig. 5, in [3]). New excess Gibbs data for RbF–LaF_3 system are presented in Eq. (9).

The same notation as proposed by Chartrand and Pelton [7,8] is kept in Eqs. (4)–(9).

$$\Delta g_{KPu/FF} = -14853.2 - 4.1840T\chi_{KPu} + (-7112.8 - 4.1840T)\chi_{PuK}\ \mathrm{J\ mol^{-1}} \quad (6)$$

$$\Delta g_{RbPu/FF} = -31587.27 + 9.4800T + (7373.95 - 7.8668T)\chi_{RbPu} + (33334.0 - 45.2400T)\chi_{PuRb}\ \mathrm{J\ mol^{-1}} \quad (7)$$

$$\Delta g_{CsPu/FF} = -21625.1 + (-1398.3 - 14.2328T)\chi_{CsPu} + (-2977.6 + 4.9257T)\chi_{LaPu}\ \mathrm{J\ mol^{-1}} \quad (8)$$

$$\Delta g_{RbLa/FF} = -31587.27 + 9.4800T + (7373.95 - 7.8668T)\chi_{RbLa} + (33334.0 - 45.2400T)\chi_{LaRb}\ \mathrm{J\ mol^{-1}}. \quad (9)$$

This method is only a rough approximation of the phase diagrams, but until some experimental data are known, it is probably the best way to estimate these systems. Since the LiF–LaF_3, NaF–LaF_3, LiF–PuF_3 and NaF–PuF_3 systems have been optimized based on experimental results, we compared the obtained excess Gibbs functions of the liquid solution for both LiF–LaF_3/LiF–PuF_3 and NaF–LaF_3/NaF–PuF_3 pairs at T = 1000 K. As it can be seen in Fig. 1 the excess Gibbs functions for NaF–LaF_3/NaF–PuF_3 pair are very similar, whereas the functions for the LiF–LaF_3 is about twice as negative as the one for the LiF–PuF_3 system. However the largest deviation around X_{LiF} = 0.5 is about 1.6 kJ mol^{-1}, still within the margin of the experimental accuracy. Anyway based on this discrepancy we can estimate the accuracy of the calculated PuF_3 containing phase diagrams. The maximum expected error was found ±33 K in temperature and 6 mol% in composition. Both values are fair enough and confirm that the extrapolation of the excess Gibbs data from LaF_3 containing systems into the PuF_3 containing systems can be justified.

Table 3
Cation–cation coordination numbers of the liquid

A	B	Z^A_{AB}	Z^B_{AB}
Li	Li	6	6
Na	Na	6	6
K	K	6	6
Rb	Rb	6	6
Cs	Cs	6	6
La	La	6	6
Pu	Pu	6	6
Li	Pu	2	6
Na	Pu	2	6
K	Pu	3	6
Rb	Pu	2	6
Cs	Pu	6	9
La	Pu	6	6

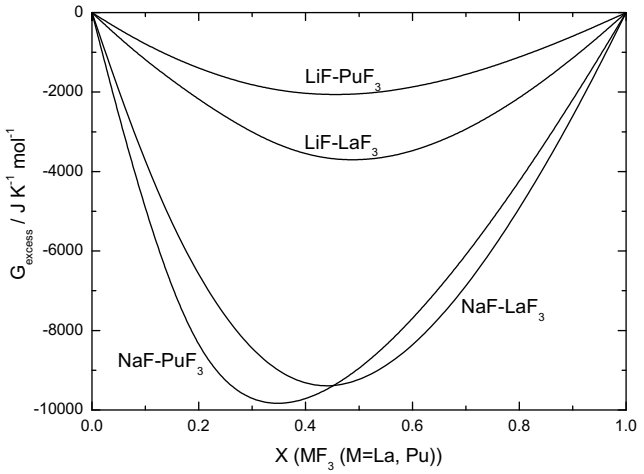

Fig. 1. Comparison of the excess Gibbs functions in LiF–LaF_3, LiF–PuF_3, NaF–LaF_3 and NaF–PuF_3 systems at T = 1000 K.

2.3. Solid solutions

The only solid solution considered in this work is in the LaF_3–PuF_3 system, which is expected to be a continuous solution since both compounds have the same crystal structure in the solid state and have very close atomic radii. This solid solution has been treated ideally, similarly as the (La,Pu)F_3 liquid solution discussed in Section 2.2.

2.4. Ternary assessments

All the ternary systems containing PuF_3 presented in this study have been extrapolated according to Kohler–Toop formalism [11]. Two groups of asymmetry are presented. The first group contains alkali halide fluorides that most likely form strongly ionic liquids. On the other hand LaF_3 and PuF_3 are compounds that rather form molecular species in the liquid and therefore belong to the second group.

Due to the lack of experimental data most of the ternary phase diagrams have been derived based only on the extrapolation from

the binary subsystems without the use of the additional ternary excess Gibbs terms. Nevertheless in case of the LiF–NaF–PuF_3 and LiF–CsF–PuF_3 systems some ternary excess Gibbs terms have been introduced. Their values (Eqs. (10), (11)) correspond to the previously described LiF–NaF–LaF_3 and LiF–CsF–LaF_3 systems [4,12] that are considered as 'proxy' systems.

$$g^{001}_{\mathrm{LiNa(Pu)/FF}} = -9565.5\ \mathrm{J\ mol^{-1}} \quad (10)$$

$$g^{001}_{\mathrm{LiCs(Pu)/F}} = -29525.5\ \mathrm{J\ mol^{-1}}. \quad (11)$$

3. Results

3.1. Binary systems

As it was discussed above, the only two binary systems optimized in this work based on known experimental data were LiF–PuF_3 and NaF–PuF_3. Both systems have also been evaluated by van der Meer et al. [6] using the classical polynomial model. Very good agreement between both results has been found and for the phase diagrams we refer to previous study [6].

The other four binary phase diagrams (KF–PuF_3,RbF–PuF_3, CsF–PuF_3 and LaF_3–PuF_3) presented in this study have been estimated based on the data from the proxy systems containing LaF_3 [3,4]. The resulting phase diagrams are shown in Fig. 2.

It is worth to compare the KF–PuF_3, RbF–PuF_3 and CsF–PuF_3 systems with the analogue systems of LaF_3. In all three cases similar shape of the liquidus has been found. Slight difference has been found in case of KF–PuF_3 where congruent melting of the K_3PuF_6 intermediate compound instead of peritectic melting as observed in the KF–LaF_3 system has been found (note that the thermodynamic data for all of the plutonium containing intermediate compounds have been estimated based on the data of the lanthanum containing proxy compounds). In the RbF–PuF_3 system the Rb_2PuF_5 and $RbPu_2F_7$ compounds are not stable whereas in the RbF–LaF_3 system the proxy Rb_2LaF_5 and $RbLa_2F_7$ compounds are stable [3], though only with a very narrow field of stability having a marginal influence on the shape of the liquidus. It is thus expected that the absence of the Rb_2PuF_5 and $RbPu_2F_7$ compounds would not effect the melting behavior of the higher order systems significantly.

All the calculated invariant equilibria in the above-mentioned binaries are summarized in Table 4.

3.2. Ternary systems

All the ternary phase diagrams from the LiF–NaF–KF–RbF–CsF–LaF_3–PuF_3 system containing PuF_3 are shown in Figs. 3–17 as a projection of the liquidus surface. All the ternary invariant points with corresponding solid phases in equilibrium are listed in Table 5.

Table 4
Calculated invariant equilibria in LiF–PuF_3, NaF–PuF_3, KF–PuF_3, CsF–PuF_3 and LaF_3–PuF_3 systems

System	Equilibrium	T (K)	X_{PuF_3}
LiF–PuF_3	Eutectic	1017	0.212
NaF–PuF_3	Eutectic	999	0.221
	Peritectic	1111	0.387
KF–PuF_3	Eutectic	916	0.210
	Eutectic	892	0.349
	Peritectic	939	0.429
RbF–PuF_3	Eutectic	779	0.214
	Eutectic	799	0.262
	Peritectic	937	0.369
CsF–PuF_3	Eutectic	852	0.094
	Eutectic	882	0.437

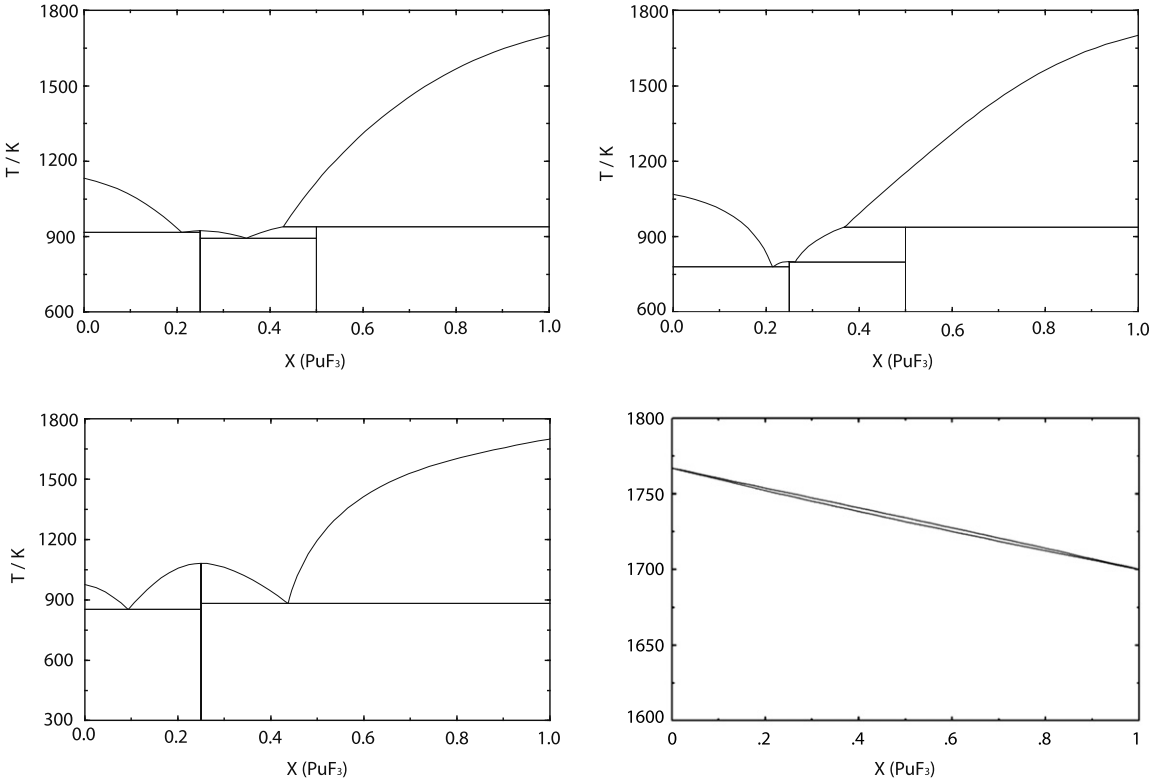

Fig. 2. Calculated phase diagrams of the KF–PuF_3 (upper left), RbF–PuF_3 (upper right), CsF–PuF_3 (bottom left) and LaF_3–PuF_3 (bottom right) systems.

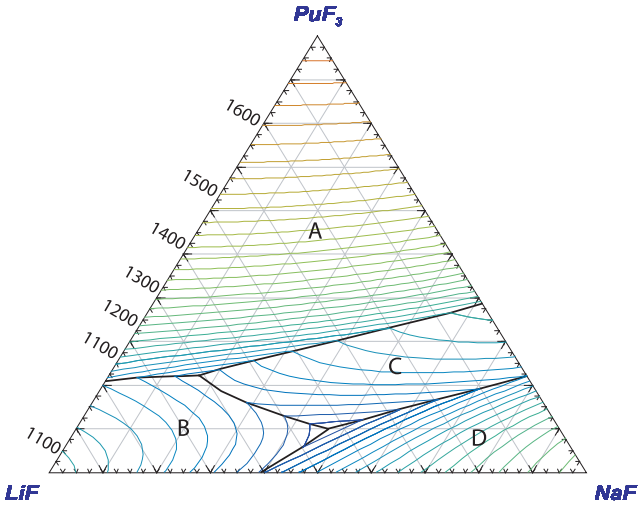

Fig. 3. Calculated liquid surface of LiF–NaF–PuF_3. Isotherms are labelled in K with interval of 25 K. Primary phase fields: (A) PuF_3; (B) (Li,Na)F; (C) $NaPuF_4$; (D) (Li,Na)F.

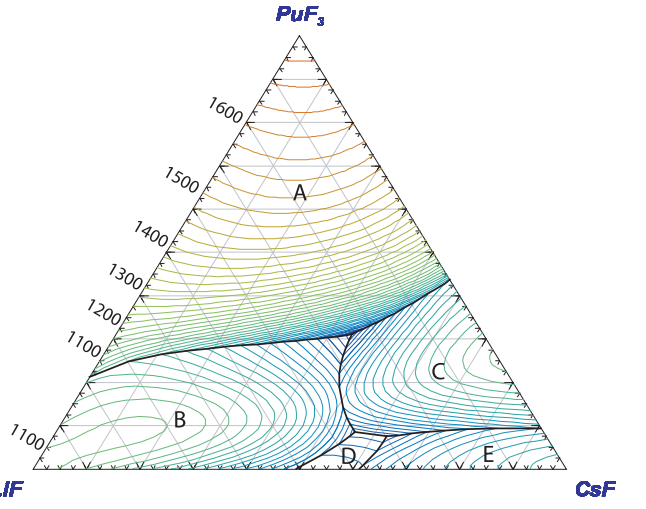

Fig. 6. Calculated liquid surface of LiF–CsF–PuF_3. Isotherms are labelled in K with interval of 25 K. Primary phase fields: (A) PuF_3; (B) LiF; (C) Cs_3PuF_6; (D) $LiCsF_2$; (E) CsF.

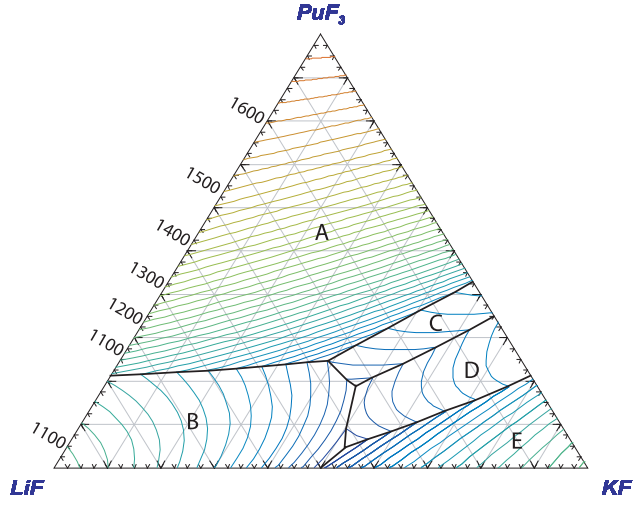

Fig. 4. Calculated liquid surface of LiF–KF–PuF_3. Isotherms are labelled in K with interval of 25 K. Primary phase fields: (A) PuF_3; (B) LiF; (C) $KPuF_4$; (D) K_3PuF_6; (E) KF.

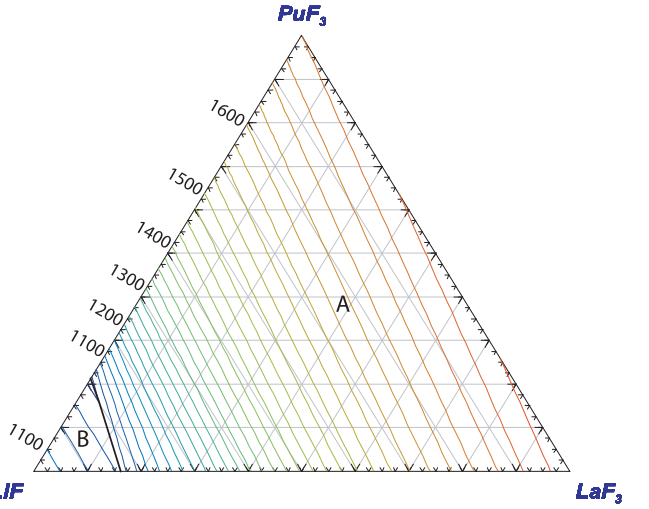

Fig. 7. Calculated liquid surface of LiF–LaF_3–PuF_3. Isotherms are labelled in K with interval of 25 K. Primary phase fields: (A) $(La,Pu)F_3$; (B) LiF.

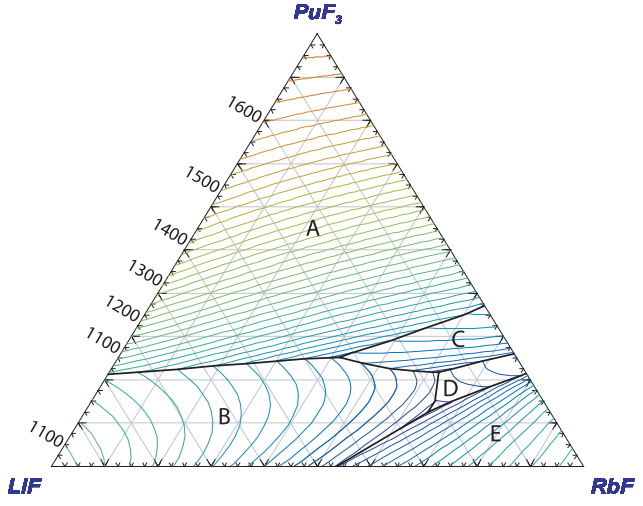

Fig. 5. Calculated liquid surface of LiF–RbF–PuF_3. Isotherms are labelled in K with interval of 25 K. Primary phase fields: (A) PuF_3; (B) LiF; (C) $RbPuF_4$; (D) Rb_3PuF_6; (E) RbF.

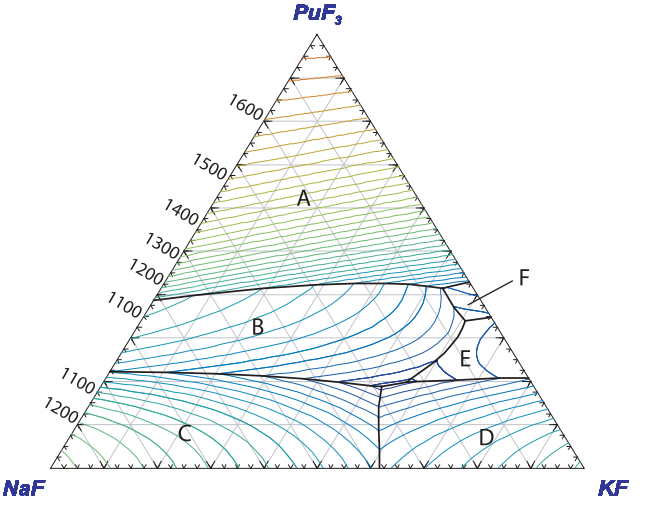

Fig. 8. Calculated liquid surface of NaF–KF–PuF_3. Isotherms are labelled in K with interval of 25 K. Primary phase fields: (A) PuF_3; (B) $NaPuF_4$; (C) NaF; (D) KF; (E) K_3PuF_6; (F) $KPuF_4$.

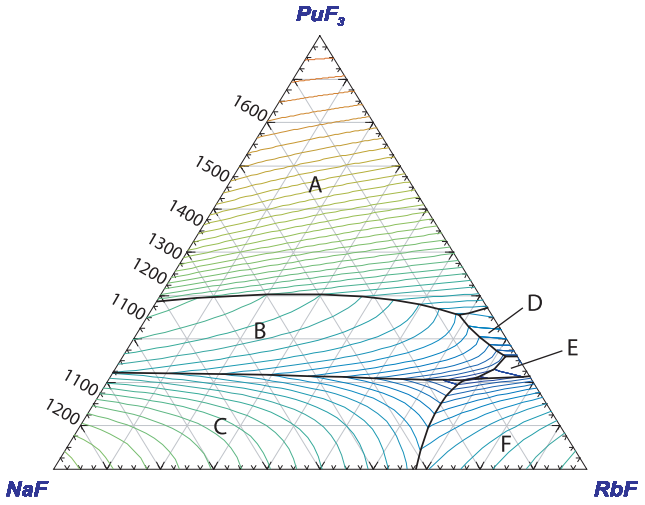

Fig. 9. Calculated liquid surface of NaF–RbF–PuF_3. Isotherms are labelled in K with interval of 25 K. Primary phase fields: (A) PuF_3; (B) $NaPuF_4$; (C) NaF; (D) $RbPuF_4$; (E) Rb_3PuF_6; (F) RbF.

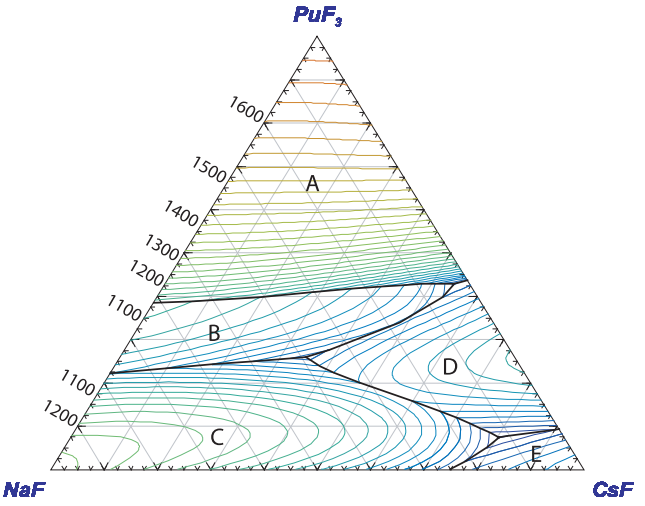

Fig. 10. Calculated liquid surface of NaF–CsF–PuF_3. Isotherms are labelled in K with interval of 25 K. Primary phase fields: (A) PuF_3; (B) $NaPuF_4$; (C) NaF; (D) Cs_3PuF_6; (E) CsF.

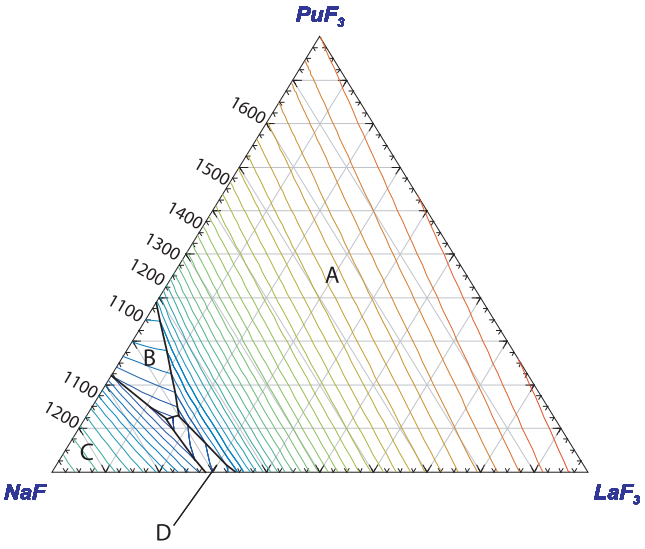

Fig. 11. Calculated liquid surface of NaF–LaF_3–PuF_3. Isotherms are labelled in K with interval of 25 K. Primary phase fields: (A) $(La,Pu)F_3$; (B) $NaPuF_4$; (C) NaF; (D) $NaLaF_4$.

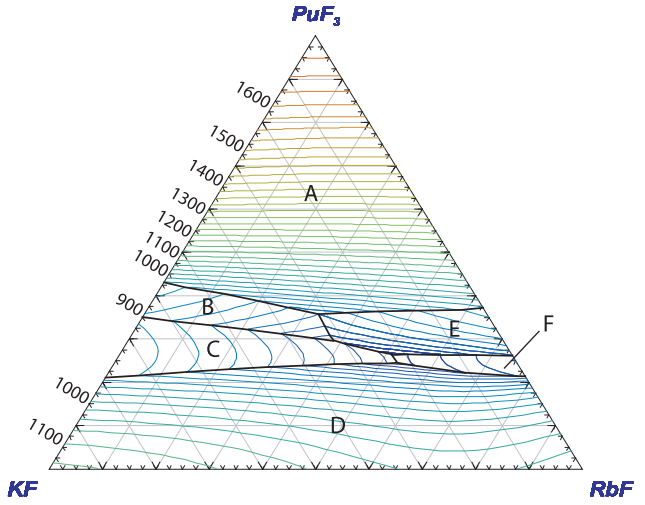

Fig. 12. Calculated liquid surface of KF–RbF–PuF_3. Isotherms are labelled in K with interval of 25 K. Primary phase fields: (A) PuF_3; (B) $KPuF_4$; (C) K_3PuF_6; (D) (K,Rb)F; (E) $RbPuF_4$; (F) Rb_3PuF_6.

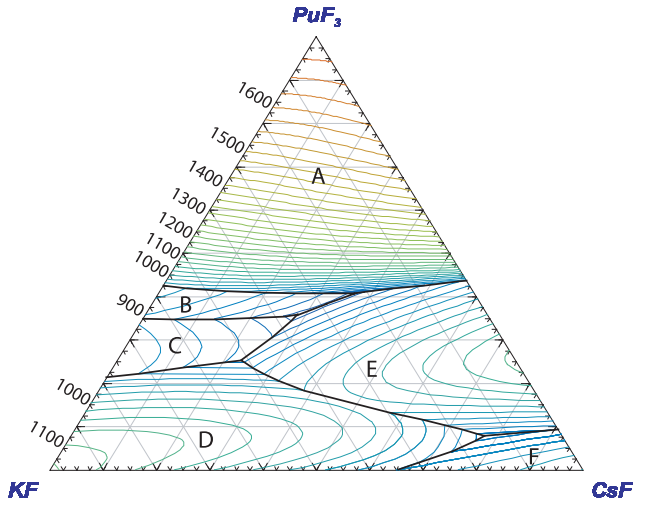

Fig. 13. Calculated liquid surface of KF–CsF–PuF_3. Isotherms are labelled in K with interval of 25 K. Primary phase fields: (A) PuF_3; (B) $KPuF_4$; (C) K_3PuF_6; (D) (K,Cs)F; (E) Cs_3PuF_6; (F) (K,Cs)F.

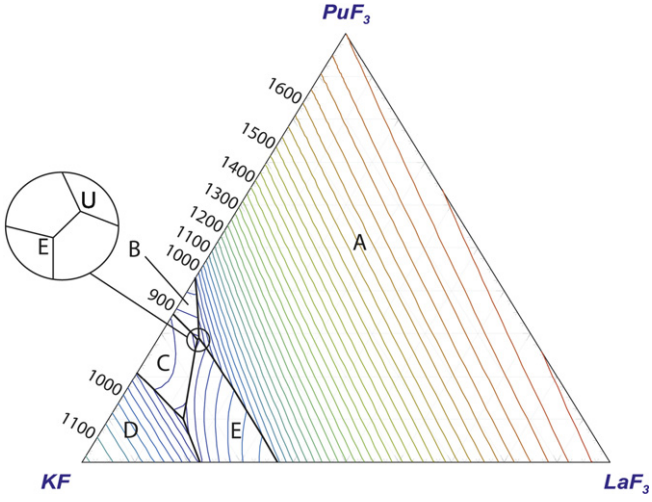

Fig. 14. Calculated liquid surface of KF–LaF_3–PuF_3. Isotherms are labelled in K with interval of 25 K. Primary phase fields: (A) $(La,Pu)F_3$; (B) $KPuF_4$; (C) K_3PuF_6; (D) KF; (E) $KLaF_4$.

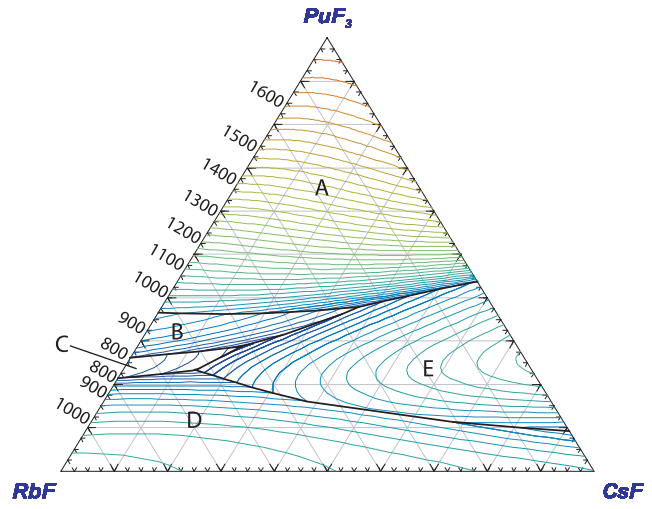

Fig. 15. Calculated liquid surface of RbF–CsF–PuF_3. Isotherms are labelled in K with interval of 25 K. Primary phase fields: (A) PuF_3; (B) $RbPuF_4$; (C) Rb_3PuF_6; (D) (Rb,Cs)F; (E) Cs_3PuF_4.

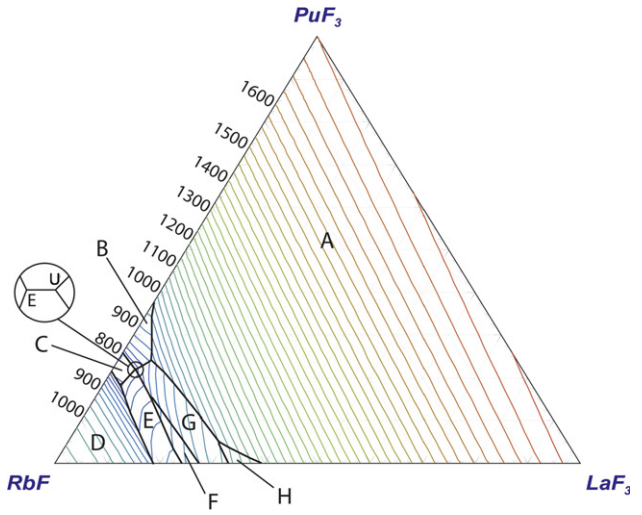

Fig. 16. Calculated liquid surface of RbF–LaF_3–PuF_3. Isotherms are labelled in K with interval of 25 K. Primary phase fields: (A) (La,Pu)F; (B) $RbPuF_4$; (C) Rb_3PuF_6; (D) RbF; (E) Rb_3LaF_6; (F) Rb_2LaF_5; (G) $RbLaF_4$; (H) $RbLa_2F_7$.

4. Potential actinide burner fuel compositions

In the report by Zherebtsov and Ignatiev [13] the MOlten Salt Actinide Recycler and Transmuter (MOSART) system has been introduced. It is actually a nuclear reactor with a fast neutron spectrum that uses PuF_3 as a fissile material. The big benefit of this system is that some amount of transuranium actinides (long lived isotopes coming from nuclear waste) can be added to the fuel in order to transmute them into short lived isotopes. The fuel of MOSART concept is based on the LiF–NaF–BeF_2 matrix (15–58–27 mol%), in which PuF_3 and some higher actinides of total concentration 1.3 mol% are dissolved.

One of the aims of the present study was to optimize the fuel choice based on the MOSART concept using only alkali fluorides for the matrix, thus avoiding BeF_2. It is not only because of its toxicity, but also better solubility of the PuF_3 compound is achieved when BeF_2 is excluded.

Our goal is to find a composition in the LiF–NaF–MF (where M = K of Rb) system that contains 1.3 mol% of PuF_3 (in this study representative of all actinides), whereas LiF, NaF, KF and RbF (components for the matrix) could vary. Another criterion to be fulfilled is the melting temperature of the fuel. It must be lower than 823 K, which is 50 K (safety margin) below the design inlet temperature of the reactor in the MOSART concept [13].

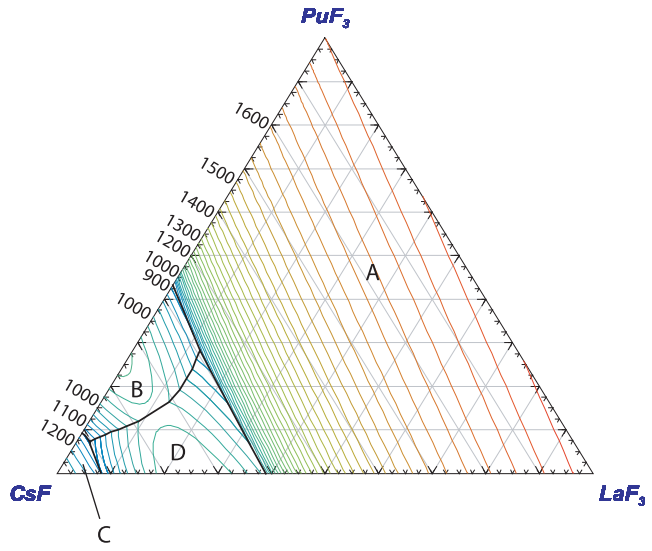

Fig. 17. Calculated liquid surface of CsF–LaF_3–PuF_3. Isotherms are labelled in K with interval of 25 K. Primary phase fields: (A) (La,Pu)F; (B) Cs_3PuF_6; (C) CsF; (D) Cs_3LaF_6.

4.1. Melting behavior

There are six ternaries containing PuF_3 in the LiF–NaF–KF–RbF–PuF_3 system. All of them are listed in Table 5 and as it can be seen, four of these (LiF–KF–PuF_3,LiF–RbF–PuF_3, NaF–RbF–PuF_3 and KF–RbF–PuF_3) systems have eutectics lower than our criterion (T = 823 K). However the compositions of PuF_3 in these systems are different from the targeted 1.3 mol%. Therefore a set of four pseudobinary phase diagrams has been calculated keeping the concentration of PuF_3 at 1.3 mol%. While in the KF–RbF–(PuF_3 = 1.3 - mol%) and NaF–RbF–(PuF_3 = 1.3 mol%) systems the lowest melting temperatures are much too high to be acceptable for Molten Salt Reactor (T = 1037 K and T = 935 K), the other two LiF–KF–(PuF_3 = 1.3 mol%) and LiF–RbF–(PuF_3 = 1.3 mol%) systems fulfill this condition and can be considered as an Actinide Burner fuel. The lowest melting points of these two systems correspond to $X_{LiF} = 0.482, X_{KF} = 0.505, X_{PuF_3} = 0.013$ and T = 760 K and $X_{LiF} = 0.439, X_{RbF} = 0.548, X_{PuF_3} = 0.013$ and T = 744 K, respectively.

It is also of interest to find potential fuel compositions containing three compounds of the matrix. Therefore we made further calculations and found that a matrix based on the ternary mixtures of LiF–NaF–RbF, LiF–NaF–KF and LiF–KF–RbF with addition of 1.3 mol% of PuF_3 have very low pseudo-ternary eutectics and these points can be considered as a fuel compositions also. The corresponding compositions and their melting points are given in Table 6.

Obviously all of the melting temperatures of the potential fuel compositions from Table 6 are significantly lower than our temperature criterion (T = 823 K), therefore three pseudoternary phase diagrams have been plotted (see Figs. 18–20) at T = 823 K in order to show the composition margin that is represented by the liquid region in these phase diagrams.

4.2. Solubility for actinides

According to our thermodynamic assessment the solubilities of PuF_3 in the mixtures of alkali fluorides have been determined for the compositions that correspond to the fuel choices proposed on

Table 5
Calculated invariant points of the ternaries containing PuF_3

System A–B–C	X_A	X_B	X_C	T (K)	Equilibrium	Solid phase present
LiF–NaF–PuF_3	0.429	0.472	0.099	877	Eutectic	(Li,Na)F (1) + (Li,Na)F (2) + $NaPuF_4$
	0.611	0.167	0.222	958	Eutectic	(Li,Na)F + PuF_3 + $NaPuF_4$
LiF–KF–PuF_3	0.431	0.522	0.047	749	Eutectic	KF + LiF + K_3PuF_6
	0.341	0.471	0.188	786	Eutectic	$KPuF_4$ + LiF + K_3PuF_6
	0.364	0.390	0.246	825	Quasi-peritectic	$KPuF_4$ + LiF + PuF_3
LiF–RbF–PuF_3	0.228	0.645	0.126	713	Eutectic	LiF + Rb_3PuF_6 + RbF
	0.163	0.618	0.218	741	Eutectic	LiF + Rb_3PuF_6 + $RbPuF_4$
	0.332	0.416	0.252	841	Quasi-peritectic	LiF + $RbPuF_4$ + PuF_3
LiF–CsF–PuF_3	0.246	0.443	0.311	631	Eutectic	LiF + Cs_3PuF_6 + PuF_3
	0.299	0.626	0.075	678	Eutectic	CsF + Cs_3PuF_6 + $LiCsF_2$
	0.354	0.560	0.085	681	Eutectic	LiF + Cs_3PuF_6 + $LiCsF_2$
LiF–LaF_3–PuF_3	0.788	0.000	0.212	631	Minimum	
NaF–KF–PuF_3	0.285	0.528	0.187	840	Eutectic	(Na,K)F (1) + (Na,K)F (2) + $NaPuF_4$
	0.234	0.568	0.198	843	Quasi-peritectic	(Na,K)F + K_3PuF_6 + $NaPuF_4$
	0.053	0.608	0.340	878	Eutectic	$KPuF_4$ + K_3PuF_6 + $NaPuF_4$
	0.058	0.528	0.414	922	Quasi-peritectic	PuF_3 + $KPuF_4$ + $NaPuF_4$
NaF–RbF–PuF_3	0.104	0.687	0.209	741	Eutectic	Rb_3PuF_6 + RbF + $NaPuF_4$
	0.131	0.666	0.203	748	Quasi-peritectic	NaF + RbF + $NaPuF_4$
	0.023	0.717	0.260	791	Quasi-peritectic	$RbPuF_4$ + Rb_3PuF_6 + $NaPuF_4$
	0.062	0.582	0.356	920	Quasi-peritectic	PuF_3 + $NaPuF_4$ + $RbPuF_4$
NaF–CsF–PuF_3	0.122	0.803	0.075	821	Eutectic	NaF + CsF + Cs_3PuF_6
	0.029	0.541	0.430	871	Eutectic	PuF_3 + $NaPuF_4$ + Cs_3PuF_6
	0.391	0.349	0.260	888	Eutectic	NaF + $NaPuF_4$ + Cs_3PuF_6
NaF–LaF_3-PuF_3	0.726	0.153	0.121	964	Eutectic	NaF + $NaPuF_4$ + $NaLaF_4$
	0.699	0.171	0.130	984	Quasi-peritectic	(La,Pu)F_3 + $NaPuF_4$ + $NaLaF_4$
KF–RbF–PuF_3	0.225	0.512	0.264	713	Eutectic	K_3PuF_6 + Rb_3PuF_6 + $RbPuF_4$
	0.225	0.530	0.245	714	Eutectic	K_3PuF_6 + (*K,Rb*)F + Rb_3PuF_6
	0.318	0.385	0.297	758	Quasi-peritectic	$KPuF_4$ + K_3PuF_6 + $RbPuF_4$
	0.317	0.326	0.357	826	Quasi-peritectic	PuF_3 + $KPuF_4$ + $RbPuF_4$
KF–CsF–PuF_3	0.356	0.286	0.358	789	Eutectic	Cs_3PuF_6 + $KPuF_4$ + K_3PuF_6
	0.223	0.369	0.408	792	Eutectic	Cs_3PuF_6 + PuF_3 + $KPuF_4$
	0.515	0.231	0.254	840	Quasi-peritectic	Cs_3PuF_6 + K_3PuF_6 + (K,Cs)F
	0.145	0.776	0.079	835	Eutectic	Cs_3PuF_6 + (K,Cs)F (1) + (K,Cs)F (2)
KF–LaF_3-PuF_3	0.638	0.075	0.286	869	Eutectic	$KLaF_4$ + $KPuF_4$ + K_3PuF_6
	0.633	0.077	0.290	873	Quasi-peritectic	$KLaF_4$ + $KPuF_4$ + (La,Pu)F_3
	0.759	0.140	0.100	861	Eutectic	$KLaF_4$ + K_3PuF_6 + KF
RbF–CsF–PuF_3	0.632	0.135	0.233	723	Eutectic	(Rb,Cs)F + Cs_3PuF_6 + Rb_3PuF_6
	0.518	0.194	0.288	713	Eutectic	$RbPuF_4$ + Cs_3PuF_6 + Rb_3PuF_6
	0.251	0.370	0.379	777	Quasi-peritectic	$RbPuF_4$ + Cs_3PuF_6 + PuF_3
RbF–LaF_3-PuF_3	0.784	0.033	0.183	767	Eutectic	RbF + Rb_3LaF_6 + Rb_3PuF_6
	0.737	0.044	0.220	783	Eutectic	$RbPuF_4$ + Rb_3PuF_6 + $RbLaF_4$
	0.736	0.044	0.219	784	Quasi-peritectic	$RbPuF_4$ + Rb_3LaF_6 + $RbLaF_4$
	0.740	0.104	0.156	845	Quasi-peritectic	Rb_2LaF_5 + Rb_3LaF_5 + $RbLaF_4$
	0.695	0.062	0.242	857	Quasi-peritectic	$RbPuF_4$ + (La,Pu)F_3 + $RbLaF_4$
	0.663	0.287	0.051	999	Quasi-peritectic	Rb_2LaF_5 + (La,Pu)F_3 + $RbLaF_4$
CsF–LaF_3-PuF_3	0.903	0.024	0.073	845	Eutectic	CsF + Cs_3LaF_6 + Cs_3PuF_6
	0.592	0.126	0.282	902	Eutectic	(La,Pu)F_3 + Cs_3PuF_6 + Cs_3LaF_6

Table 6
Potentional compositions for Actinide Burner fuel, their melting temperatures, vapor pressures at T = 988 K (outlet temperature of the MOSART concept) and the boiling temperatures

Composition (mol%)	$T_{melting}$/K	p_{vapor}/Pa at T = 988 K	$T_{boiling}$/K
LiF–KF–PuF_3 (0.482–0.505–0.013)	760	0.8	1917
LiF–RbF–PuF_3 (0.439–0.548–0.013)	744	3.5	1839
LiF–NaF–RbF–PuF_3 (0.395–0.140–0.452–0.013)	706	3.2	1926
LiF–NaF–KF–PuF_3 (0.433–0.140–0.414–0.013)	723	0.7	1937
LiF–KF–RbF–PuF_3 (0.428–0.188–0.371–0.013)	711	2.8	1863

a basis of the melting behavior (see Table 6). The solubilities for a chosen matrix composition are reported in Table 1 as a functions of temperature.

4.3. Vapor pressure

Based on the melting behavior we have found five potential fuel compositions. Using the thermodynamic data of all the relevant gas species, we calculated their vapor pressures at T = 988 K. This temperature is the outlet temperature of the reactor based on the MOSART concept [13]. The calculated values (summarized in Table 6) are very low, thus acceptable for the molten salt reactor. The boiling temperatures related to each of the fuel choices are listed in Table 6 as well.

4.4. Influence of the fission products

Our studied system contains also CsF and LaF_3. As was mentioned in Section 1 these compounds are considered as fission products that are very difficult to separate from the fuel during the clean-up treatment and their accumulation is expected.

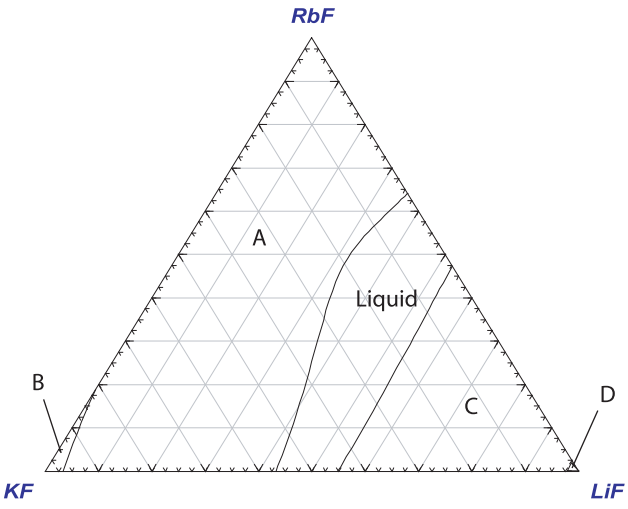

Fig. 18. Pseudoternary plot of the LiF–KF–RbF–PuF_3 system with constant amount of PuF_3 = 1.3 mol% at T = 823 K. Phases in equilibrium: (A) (K,Rb)F + L; (B) K_3PuF_6 + (K,Rb)F + L; (C) LiF + L; (D) LiF + PuF_3 + L; L – Liquid.

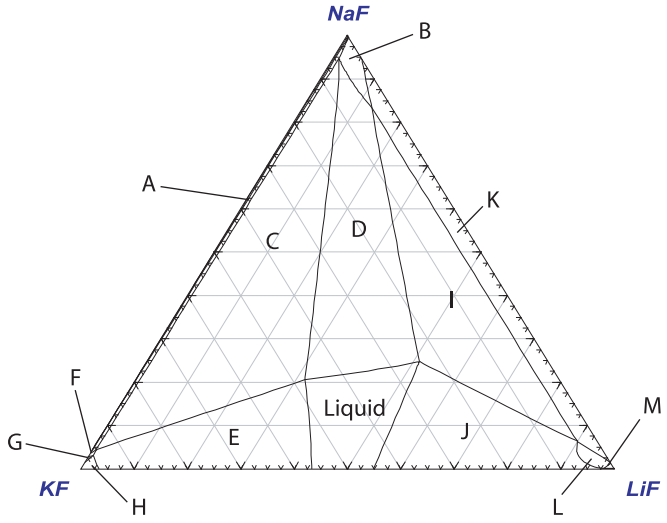

Fig. 19. Pseudoternary plot of the LiF–NaF–KF–PuF_3 system with constant amount of PuF_3 = 1.3 mol% at T = 823 K. Phases in equilibrium: (A) $NaPuF_4$ + (Na,K)F + (Li,Na)F + L; (B) $NaPuF_4$ + (Li,Na)F + L; (C) (Li,Na)F + (Na,K)F + L; (D) (Li,Na)F + L; (E) (Na,K)F + L; (F) $NaPuF_4$ + (Na,K)F + L; (G) $NaPuF_4$ + (Na,K)F + K_3PuF_6 + L; (H) K_3PuF_6 + (Na,K)F + L; (I) LiF + (Li,Na)F+L; (J) LiF + L; (K) $NaPuF_4$ + (Li,Na)F + LiF + L; (L) $NaPuF_4$ + LiF + L; (M) $NaPuF_4$ + LiF + PuF_3 + L; L – Liquid.

Nevertheless even the amounts of CsF and LaF_3 accumulated in the fuel cycle after 30 years operation (0.06 mol% of CsF and 0.37 mol% of LaF_3 [14]) are relatively low and as was confirmed by the calculations, they negligibly affect the melting behavior and vaporization of the fuel.

5. Summary

Based on our thermodynamic assessment we have found five potential fuel compositions that show good melting behavior, and low vapor pressure at the operating temperature of the Molten Salt Reactor (MOSART concept). Moreover the composition margins were presented, that can be useful in the search for an optimal fuel choice when considering other relevant properties (viscosity, heat capacity, thermal conductivity, etc.) that are still matter of further investigation. The solubilities of actinides in the matrixes corresponding to the fuel choices have been calculated and relatively high values have been found.

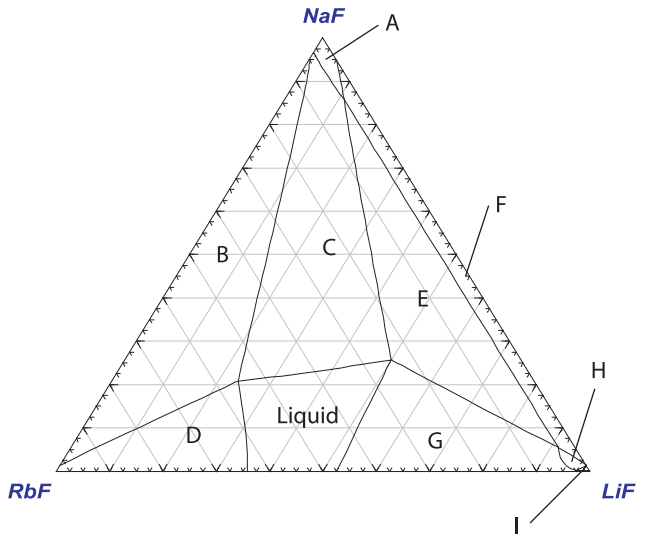

Fig. 20. Pseudoternary plot of the LiF–NaF–RbF–PuF_3 system with constant amount of PuF_3 = 1.3 mol% at T = 823 K. Phases in equilibrium: (A) (Li,Na)F + $NaPuF_4$ + L; (B) (Li,Na)F + RbF + L; (C) (Li,Na)F + L; (D) RbF + L; (E) (Li,Na)F + LiF + L; (F) $NaPuF_4$ + (Li,Na)F + LiF + L; (G) LiF + L; (H) LiF + $NaPuF_4$ + L; (I) LiF + PuF_3 + $NaPuF_4$ + $RbPuF_4$; L – Liquid.

Acknowledgement

O.B. acknowledges the European Commission for support given in the frame of the program 'Training and Mobility of Researchers'.

References

[1] C.J. Barton, J. Chem. Phys. 32 (1960) 1150.
[2] J.C. Mailen, F.J. Smith, L.M. Ferris, J. Chem. Eng. Data 16 (1971) 68.
[3] O. Benes, J.P.M. van der Meer, R.J.M. Konings, Comput. Coupling Phase Diagrams Thermochem. 31 (2007) 209.
[4] O. Benes, R.J.M. Konings, Comput. Coupling Phase Diagrams Thermochem. 32 (2008) 121.
[5] R.J.M. Konings, J.P.M. van der Meer, E. Walle, Chemical aspects of Molten Salt Reactor Fuel, Tech. Rep., ITU-TN 2005/25, 2005.
[6] J.P.M. van der Meer, R.J.M. Konings, K. Hack, H.A.J. Oonk, Chem. Mater. 18 (2006) 510.
[7] A.D. Pelton, P. Chartrand, G. Eriksson, Metall. Trans. 32A (2001) 1409.
[8] P. Chartrand, A.D. Pelton, Metall. Trans. 32A (2001) 1397.
[9] C.J. Barton, R.A. Strehlow, J. Inorg. Nucl. Chem. 18 (1961) 143.
[10] C.J. Barton, J.D. Redman, R.A. Strehlow, J. Inorg. Nucl. Chem. 20 (1961) 45.
[11] A.D. Pelton, Calphad 25 (2001) 319.
[12] O. Benes, R.J.M. Konings, J. Alloys Compd. 452 (2008) 110.
[13] A.L. Zherebtsov, V.V. Ignatiev, Experimental Mock-Up of Accelerator-Based Facility for Transmutation of Radioactive Waste and Conversion of Military Plutonium, Tech. Rep., Nr. 1606 Annual Report, 2006.
[14] Status of small reactor designs without on-site refuelling, Tech. Rep., IAEA-TECDOC-1536, 2007.
[15] R.J.M. Konings, L.R. Morss, J. Fuger, The Chemistry of the Actinide and Transactinide Elements, vol. 4, Springer, Dordrecht, The Netherlands, 2006. (Chapter 19).
[16] M.W. Chase Jr. (Ed.), NIST-JANAF Thermochemical Tables Fourth Edition, J. Phys. Chem. Ref. Data, Monograph, vol. 9, 1998.